CHALMERS

Conceptual Gas Turbine Modelling for Oxy-fuel Power Cycles

EGILL MARON THORBERGSSON

Department of Applied Mechanics
CHALMERS UNIVERSITY OF TECHNOLOGY
Gothenburg, Sweden 2012

THESIS FOR THE DEGREE OF LICENTIATE OF ENGINEERING
IN
THERMO AND FLUID DYNAMICS

Conceptual Gas Turbine Modelling for Oxy-fuel Power Cycles

EGILL MARON THORBERGSSON

Department of Applied Mechanics
CHALMERS UNIVERSITY OF TECHNOLOGY

Gothenburg, Sweden 2012

Conceptual Gas Turbine Modelling for
Oxy-fuel Power Cycles
EGILL MARON THORBERGSSON

Thesis for the degree of Licentiate of Engineering 2012:06
ISSN 1652-8565
Department of Applied Mechanics
Chalmers University of Technology
SE-412 96 Gothenburg
Sweden
Telephone: +46 (0)31-772 1000

Chalmers Reproservice
Gothenburg, Sweden 2012

Conceptual Gas Turbine Modelling for Oxy-fuel Power Cycles
Thesis for the degree of Licentiate of Engineering in Thermo and Fluid Dynamics
EGILL MARON THORBERGSSON
Department of Applied Mechanics
Chalmers University of Technology

Abstract

The electricity consumption in the world is growing at an ever increasing rate. Today's electricity generation is highly dependent on combustion of fossil fuel. This leads to emissions of carbon dioxide into the atmosphere. Increased atmospheric CO_2 concentration results in higher average surface temperature and climate change.

A short- and medium term method to decrease the carbon dioxide emissions is carbon capture and storage. This method captures carbon dioxide from point sources of emissions and then stores the carbon dioxide in geological formations. In this thesis two different types of combined cycles that are well suited for carbon capture and storage are introduced and analysed. The cycles are the Graz cycle and the Semi Closed Oxy-fuel Combustion Cycle (SCOC-CC). The net power output of the conceptual designs analysed here are around 100 MW, which is in the mid-size power output range. The simulation of the two cycles shows promising results and high efficiencies. The Graz cycle net efficiency is around 49% and the SCOC-CC net efficiency is around 46%.

The combustion in the cycles takes place using only oxygen as oxidizer instead of air. The combustion products will mainly be steam and carbon dioxide. This influences the properties of the working media in the gas turbines used in the cycles. Traditional design tools for the gas turbine therefore needs modification. The thesis describes the conceptual design tool used to design the compressor part of the gas turbines. The tool is based on a one dimensional model that uses empirical data to compute losses. The thesis also describes the development of a two dimensional compressor design method.

Two different layouts of the gas turbine were studied for the SCOC-CC, a one shaft configuration and a two shaft configuration. The one shaft configuration resulted in a compressor design that was relative bulky, with 18 stages. The two shaft configuration resulted in a more favourable compressor design with 14 stages.

The design of the gas turbine for the Graz cycle has both benefits and disadvantages originating from the fact the working fluid in the Graz cycle has a higher fraction of steam compared to the SCOC-CC. This difference in the working fluid will result in that the turbomachinery will be smaller for the Graz cycle compared to the SCOC-CC. This however also results in that the heights of the blades in the rear stages of the compressor will be relatively small. This will result in a higher amount of losses generated in the rear stages. The preferred Graz cycle gas turbine configuration is a compressor geared intercooled design.

Keywords: Carbon capture and storage, oxy-fuel combustion combined cycles, Graz cycle, Semi-closed Oxy-fuel Combustion Combined Cycle, conceptual compressor design

Acknowledgements

Takk! - Tack! - Thanks!

I would like to add some words to express gratitude at this half way on my path towards the degree Doctor of Philosophy.

The deepest gratitude goes to my supervisor Tomas Grönstedt. His understanding of the world of gas turbines and fruitful discussion has helped me to bring this thesis to a higher level.

There have been many more that have helped me along the way, and I can only list those who have helped me most substantially. I would like to thank Thomas G. Johansson for the discussions about two dimensional compressor design. I would also like to thank Xu Lei for the cooperation and discussions about the one-dimensional compressor code. My colleges at Lund University, Magnus Genrup, Klas Jonshagen and Majed Sammak, get special thanks for the discussions and collaboration in the cycle studies and the turbomachinery design. Mats Sjödin and Adrian Dahlquist at Siemens Industrial Turbomachinery in Finspang receive thanks for helpful discussions.

My colleagues and friends at the division Fluid Dynamics, receive a warm gratitude for making it a pleasure to show up to work. Morover, the administrative support by Ulla Lindberg-Thieme and Monica Vargman is gratefully acknowledged.

Finally I want to give a shout-out to my fiancée Sigríður, for being by my side in this roller coaster that we call life.

This research has been funded by the Swedish Energy Agency, Siemens Industrial Turbomechinery AB, Volvo Aero Corporation and the Royal Institute of Technology through the Swedish research program TURBOPOWER. The support of which is gratefully acknowledged.

Egill Maron Thorbergsson
March 8, 2012
Gothenburg

Nomenclature

Abbreviations

HRSG	Heat Recovery Steam Generator
SCOC-CC	Semi-closed Oxy-fuel Combustion Combined Cycle

Latin symbols

c	absolute speed, blade chord
D_{eq}	equivalent diffusion factor
DF	diffusion factor
H	stagnation enthalpy
h	static enthalpy
i	incidence angle
M	Mach number
$\dot{m}$	mass flow
m	coefficient for camber and space/chord ratio
R	degree of reaction
r	coordinate in radial direction, radius
s	blade pitch
t	blade thickness
U	blade velocity
W_x	shaft work
w	relative velocity
x	coordinate in axial direction

Greek symbols

α	absolute flow angle
β	relative flow angle
δ	deviation angle
ε	blade tip clearance
ζ	blade stagger angle
θ	blade camber angle
κ	blade angle
ρ	density
ψ	stage loading coefficient
ω	loss coefficient

Subscripts

1	cascade inlet
2	cascade exit
ew	end wall
ml	minimum loss
p	profile
θ	coordinate in tangential direction

Thesis

This thesis consists of an extended summary and the following appended papers:

Paper A M. Sammak, K. Jonshagen, M. Thern, M. Genrup, E. Thorbergsson, and T. Grönstedt. Conceptual Design of a Mid-Sized, Semi-closed oxy-fuel combustion combined cycle. *ASME Turbo Expo 2011: Power for Land, Sea and Air, 6-10 June* (2011)

Paper B Egill Thorbergsson and Tomas Grönstedt. Multicriteria Optimization of Conceptual Compressor Aerodynamic Design. *20th International Society for Airbreathing Engines* (2011)

Paper C M. Sammak, M. Genrup, E. Thorbergsson, and T. Grönstedt. Single and Twin-Shaft Oxy-Fuel Gas Turbine Design in a Mid-Size Semi-Closed Oxy-Fuel Combustion Combined Cycle. *ASME Turbo Expo 2012: Power for Land, Sea and Air, 11-15 June* (2012)

Paper D Egill Thorbergsson, Tomas Grönstedt, Majed Sammak, and Magnus Genrup. A Comparative Analysis of Two Competing Mid-Size Oxy-Fuel Combustion Cycles. *ASME Turbo Expo 2012: Power for Land, Sea and Air, 11-15 June* (2012)

Contents

Abstract i

Acknowledgements iii

Nomenclature v

Thesis vii

Contents ix

I Extended Summary 1

1 Introduction 3
1.1 Carbon Capture and Storage 4
1.2 Project Outline 8

2 Power Cycles 9
2.1 Cycle Simulation Tool 9
2.2 Combined Cycles 10
2.3 Oxy-fuel Combined Cycles 11

3 Conceptual Compressor Design 17
3.1 One Dimensional Design 17
3.2 Two Dimensional Design 23
3.3 Optimization 25

4 Summary of Papers 27
4.1 Paper A: Conceptual Design of a Mid-Sized, Semi-closed oxy-fuel combustion combined cycle 27
4.2 Paper B: Multicriteria Optimization of Conceptual Compressor Aerodynamic Design 27
4.3 Paper C: Single and Twin-Shaft Oxy-Fuel Gas Turbine Design in a Mid-Size Semi-Closed Oxy-Fuel Combustion Combined Cycle 28
4.4 Paper D: A Comparative Analysis of Two Competing Mid-Size Oxy-Fuel Combustion Cycles 28

References 29

A Derivation of the Radial Equilibrium Equation 35

II Appended Papers A–C 41

Part I

Extended Summary

1 Introduction

The need to decrease the anthropogenic emissions of greenhouse gases has become more important than ever before. The United Nations Climate Change Conference in Cancún in 2010 set a goal of limiting the global average temperature increase, caused by climate change, to 2°C. To accomplish this goal, the emissions of greenhouse gases needs to be decreased promptly. The International Energy Agency has stated that "action [is] needed now to sustainably enhance energy security and avert climate change" [2].

One of the major emitters of greenhouse gases is the energy sector. In 2009 this sector emitted around 65% of the world anthropogenic greenhouse gas emissions [1]. The energy sector is an even larger part of the cake in the developed countries, and was around 85% in 2008 in the European Union [7]. The main part of the sector is electricity generation. The global emission of carbon dioxide from the public electricity and heat generation was close to 12 Gt in 2009 [1].

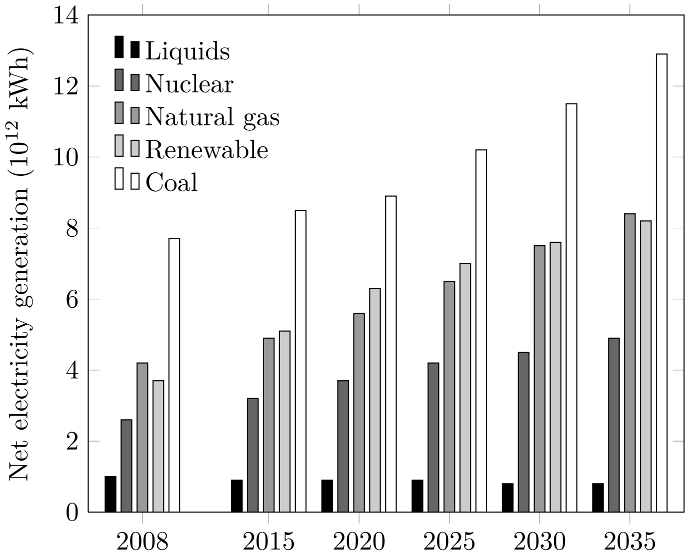

Figure 1.1: *World net electricity generation by fuel, 2008-2035 [5].*

The electricity consumption in the world is growing. The U.S. Energy Information Administration has made a projection that the world net electricity generation will increase by 84% from the level in 2008 to 2035 [5]. The projection, showing the distribution between different fuels, is shown in Figure 1.1. The assumptions used to make the prediction is that the current laws and regulations are maintained. This means that the projections do not assume any future policies that are related to limiting or reducing greenhouse gas emissions, such as caps on carbon dioxide emissions levels or taxes on carbon dioxide emissions. The projections do, however, take into account current policies that are related to renewable energy production and carbon dioxide emissions such as European Union's

"20-20-20" plan, China's wind capacity targets, and India's national solar mission. The average annual percent change over the prediction period for each fuel type is for liquids -0.9%, natural gas 2.6%, coal 1.9%, nuclear 2.4% and renewables 3.1%. The fastest growing source is the renewable energy, where the major contributors are hydroelectric and wind power. The second fastest growing fuel source for electricity generation is natural gas, where unconventional natural gas resources are helping to keep the global markets supplied and prices at competitive levels. The nuclear power increase is slightly behind the natural gas but the prediction does not reflect on the possible ramifications of the Fukushima disaster. The disaster is likely to affect the long-term global development of nuclear power. This can be seen in that some countries have adopted new policies in response of the disaster for regulating nuclear power.

To decrease the greenhouse gas emissions from the energy sector the optimal solution would be to switch from fossil fuel use and to only use renewable energy sources such as solar and geothermal. This optimal scenario is not possible since renewable energy has not gained enough momentum and new renewable technologies can not be scaled up to produce the same amount of electricity as technologies that use fossil fuel as source. An intermediate solution to battle the climate change is therefore needed while the renewable energy technologies gain momentum.

1.1 Carbon Capture and Storage

One of the intermediate solutions to decrease the carbon dioxide emissions from the current energy system is carbon capture and storage. Other examples are fuel switching and improved efficiency. The idea behind carbon capture and storage is to capture CO_2 from point sources and to store it in geological formations, in the ocean or in mineral carbonates to avoid releasing the CO_2 into the atmosphere. The text that follows explains different capture technologies and storage methods. The summary is based on the IPCC report Carbon Dioxide Capture and Storage [17].

1.1.1 Post Combustion Capture

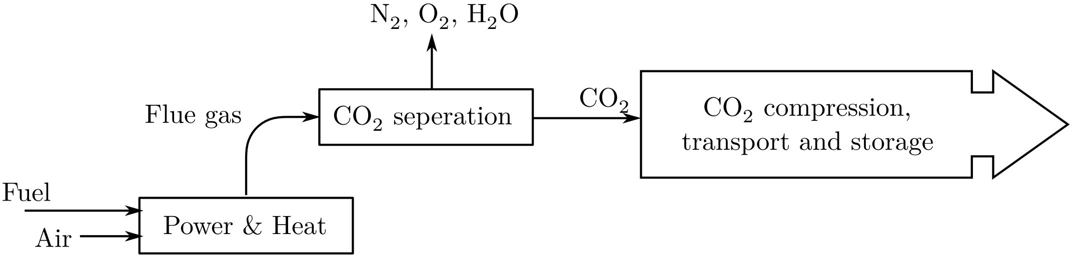

Figure 1.2: *Schematic of post combustion capture system.*

As the name suggest this method separates carbon dioxide from the flue gas after the fuel has been combusted in air. This is the combustion procedure used in most power plants today. The post combustion system is shown in a simplified schematic in Figure 1.2. The method that is the currently preferred option for post combustion CO_2 capture is a process that uses absorption based on chemical solvents. This option has reached the commercial stage of operation. Other methods are being researched that could be more cost effective such as separation with membranes, solid adsorbent, or cryogenics.

One of the advantages of the post combustion capture method is that the method can be retrofitted to an existing power plant. However, since the CO_2 contents of the flue gases are quite low, or around 3% for natural gas combined cycles to around 15% for coal-fired combustion plants the process will be quite energy intensive. The absorption process uses the reaction of an aqueous alkaline solvent to acid gas to absorb the CO_2 from the flue gas. The main energy use in the process is to heat the solvent to regenerate it, and to produce steam for the stripping. The energy is also used for liquid pumping, and for the flue gas fan.

The efficiency penalty using a post combustion capture system on a power plant typically results in an efficiency drop around ten percentage points. This number will vary depending on the percentage of CO_2 that will be recovered. The recovery for post combustion is between 80% and 95% and the exact choice for each power plant will be based on an economic trade-off.

1.1.2 Pre-combustion Capture

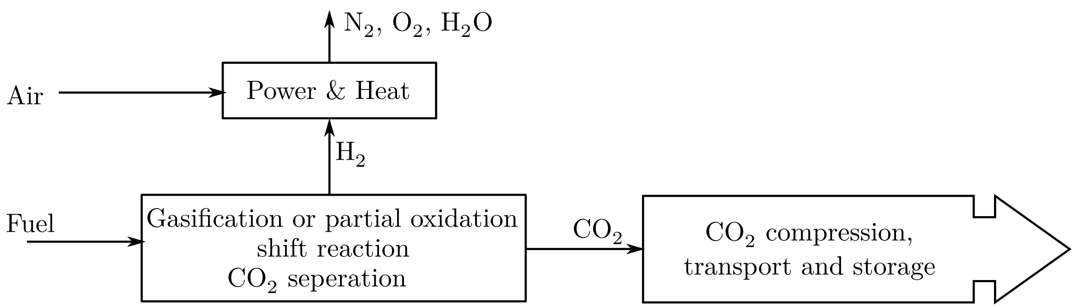

Figure 1.3: *Schematic of pre-combustion capture system.*

The pre-combustion capture method is more complex than the post-combustion method since it incorporates more processes and the power plant's combustion system needs to be redesigned. A simplified schematic of the pre-combustion system is shown in Figure 1.3. The first step in the pre-combustion method is to react the fuel with either steam or oxygen, the principle is the same in both reactions, and produce a mixture of hydrogen and carbon monoxide. When the process is applied to solid fuel it is called gasification, and when applied to gaseous and liquid fuels it is referred to as partial oxidation. The remaining CO is converted to CO_2 using steam in what is called a shift reaction. The CO_2 is then separated from the mixture of CO_2/H_2O. The CO_2 can now be compressed and sent to storage. Studies that have researched natural gas combined cycles using a pre-combustion method to capture the carbon dioxide indicate that the efficiency drop is around 8-14% [13, 21]. This can be compared to state of the art power plants that are based on natural gas combined cycles that have efficiencies around 60% [28].

1.1.3 Oxy-fuel Combustion Capture

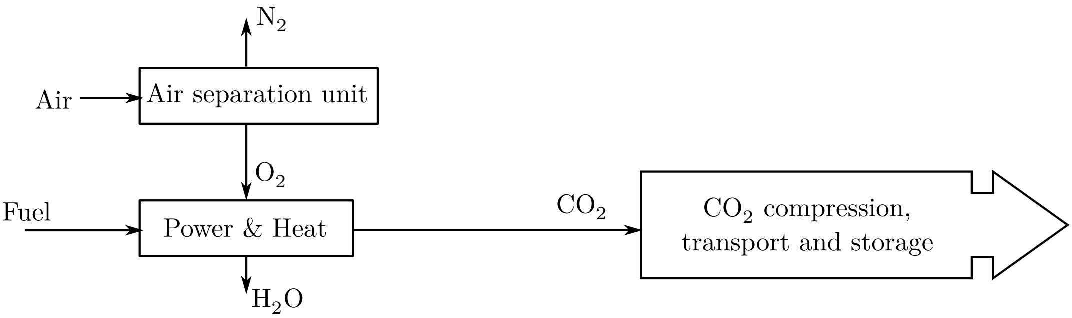

Figure 1.4: *Schematic of oxy-fuel combustion capture system.*

The oxy-fuel combustion capture method is based on using oxygen instead of air in the combustion of the fuel. The oxygen is produced using an air separation unit. The reason is to remove nitrogen from the combustion air so that the portion of nitrogen in the flue gas is negligible. The flue gas will then consist mainly of CO_2 and H_2O. The separation of the mixture is then easily done by condensing the water from the flue gas. The oxy-fuel combustion system is shown in a simplified schematic in Figure 1.4. One aspect of combustion of pure O_2 with the fuel is that the flame temperature will be high, or around 3500°C which is too high for current materials used in power plants. To cool the flame temperature flue gas can be recirculated back to the combustion chamber or water can be added. The air separation unit is usually cryogenic but novel technologies, such as membranes and chemical looping cycles are being researched.

1.1.4 Storage

An important aspect of the carbon capture and storage is the storage part. The carbon dioxide can be stored in a variety of geological settings in sedimentary basins. These basins include oil fields, depleted gas fields, deep coal seems and saline formations. These geological storages are illustrated in Figure 1.5. Researchers consider it likely that around 99% of the injected CO_2 will be retained for more than 1000 years.

The mechanisms that will store the CO_2 consists of trapping below an impermeable and confining layer, retention as an immobile phase being trapped into pore spaces of the storage formation, dissolution in the in situ formation fluids, and adsorption onto organic matter in coal and shale. Another aspect is that the CO_2 can also react with the minerals in the storage formation and confining layer to produce carbonate minerals. Additionally the CO_2 will become less mobile as time passes as a result of numerous trapping mechanisms. This will further lower the prospect of leakage.

An important factor of the storage solution part is the capacities of the storage options.

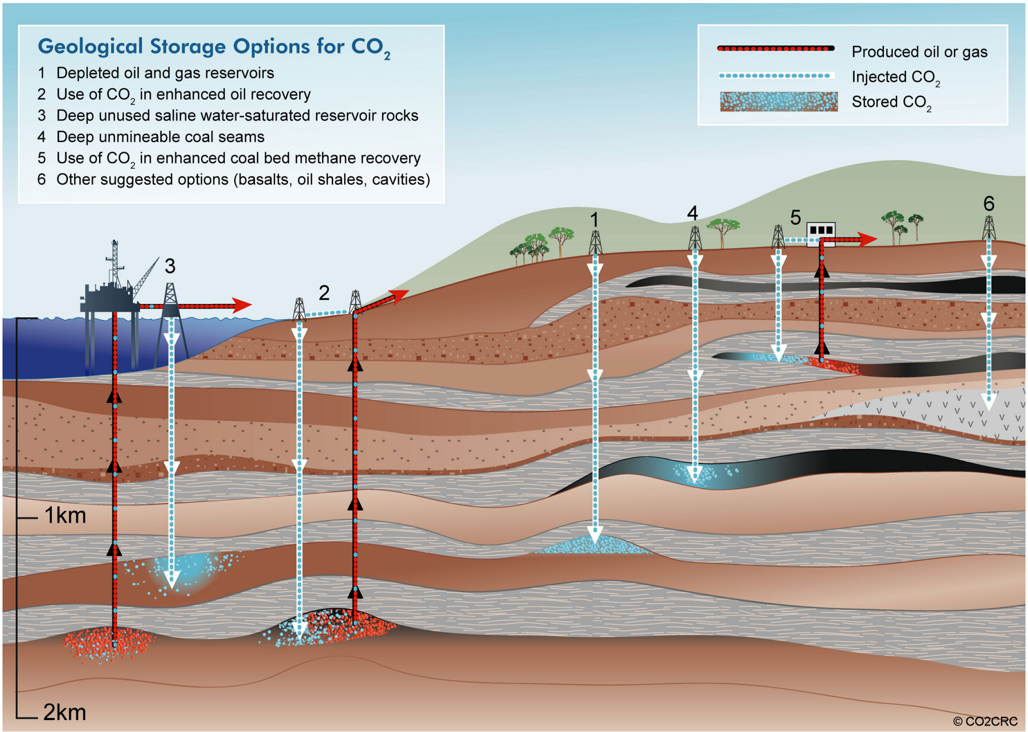

Figure 1.5: *Storage options for carbon dioxide; The options include rock formations, depleted oil and gas fields, deep saline formations and deep unmineable coal seams (Courtesy of The Cooperative Research Centre for Greenhouse Gas Technologies).*

Table 1.1: *Storage capacities of different basins in Gt CO_2, both lower and higher estimates.*

Basin	Lower	Higher
Depleted oil and gas reservoirs	675	900
Deep saline formations	1000	10000
Unminable coal formations	3	200

Researchers have estimated that the global capacity to store CO_2 underground is large, the higher estimate is around around 11 000 Gt CO_2 while the lower is around 1 700 Gt CO_2. This can be compared to the carbon dioxide emissions in 2008 from the public electricity and heat generation which was 12 Gt CO_2. The capacities for different basins are shown in Table 1.1. The location of the storage sites are likely to be distributed in the same region as many of the world's emission sources.

1.2 Project Outline

This thesis describes a project that focuses on the design of turbomachinery in oxy-fuel combustion cycles. The project is a joint project with Lund university. The project goals are to design tools that are able to design the gas turbine that are used in oxy-fuel cycles. These tools will then be used to design the turbomachinery in oxy-fuel combustion combined cycles; the Graz cycle and the Semi-closed Oxy-fuel Combustion Combined Cycle. The aim of the project is to contribute to the understanding of the opportunities and the limitations in the design of such plants. It also intends to establish computational tools and methods that can be used jointly by industry, primarily Volvo Aero and Siemens Industrial Turbomachinery, as well as by the universities involved.

2 Power Cycles

The systems or devices that are used to produce a net power output operate on thermodynamic cycles called power cycles. The most well know cycles that are used in electricity generation are the Rankine cycle, Brayton cycle, the Otto cycle and the Diesel cycle [4].

The Otto and Diesel cycles are used in reciprocating engines, and are relative small units on the order of some tens of kW to a couple of MW. The Rankine cycle is mostly used with steam as working media, and is used in coal power plants and nuclear power plants. The power cycle used in gas turbines is the Brayton cycle. This chapter focuses on the combined cycle which is a hybrid of two power cycles, using the Brayton cycle as topping cycle for the Rankine cycle.

2.1 Cycle Simulation Tool

The tool used to simulate the thermodynamic cycles is the heat and mass balance program IPSEpro, which is developed by SimTech Simulation Technology [29]. The main part of the program uses a graphical interface where the cycle components are connected. The components are either standard models that have been implemented in the software and use simple thermodynamic equations or components that the user have modelled using more advanced equations. The connection of the components establishes a system of non-linear equations. The program uses a Newton-Raphson based strategy to solve the equation system. The first step in the solution procedure is to analyse the system of equations and determine the optimal solution procedure by breaking up the equations into small groups that can be solved successively. Next phase consists of a Newton-based gradient solver that finds a solution to the equations for each group.

All components used for the work presented in this thesis uses IPSEpro standard components with the exception of the cooling flow model and the model for the combustion chamber. The model used for the cooling is a first-law thermodynamic, non-dimensional model. The model was developed and implemented by Jordal [12]. The model for the combustion chamber was devloped and implemented by Jonshagen [11].

2.1.1 Physical Properties

To calculate the physical properties of pure steam/water the cycle simulation tool uses the "Industrial Formulation 1997 for the Thermodynamic Properties of Water and Steam" data base [33]. The cycle simulation tool was linked to a state of the art thermodynamic and transport properties program, REFPROP, to calculate the physical properties of other fluids than pure steam and water. The program REFPROP is developed by National Institute of Standards and Technology [15]. The program is based on highly accurate models that are used to calculate the thermodynamic properties of pure fluids and mixtures. To calculate the thermodynamic properties of pure fluids the program uses three models: equations of state explicit in Helmholtz energy, the modified Benedict-Webb-Rubin equations of state, and an extended corresponding states model. Calculations for mixtures use a model that applies mixing rules to the Helmholtz energy of the mixture components; to account for the departure from ideal mixing it uses a departure function.

2.2 Combined Cycles

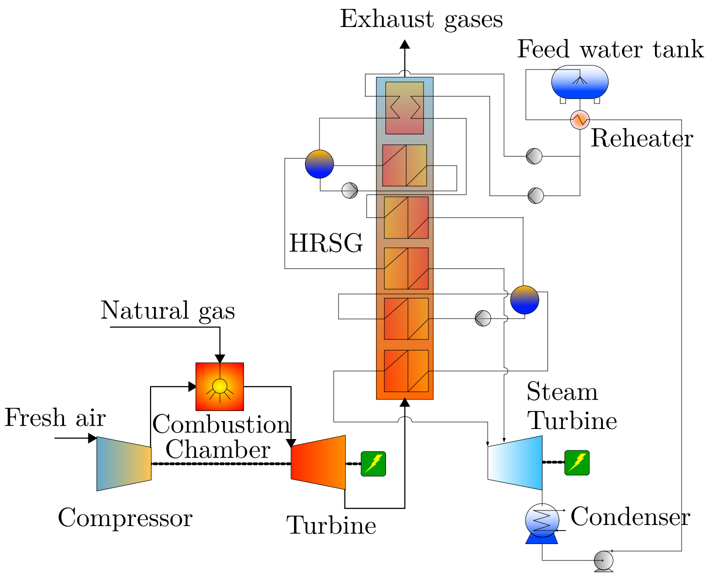

Figure 2.1: *Schematic of a combined gas/steam cycle with two pressure levels.*

A power plant that uses both a gas turbine cycle and a steam turbine cycle is called a combined gas/steam cycle or simply a combined cycle. The idea behind the combined cycle is utilizing the energy that is left in the exhaust gas after it leaves the gas turbine. The temperature of the exhaust gas from the gas turbine is in the range of 450°C to 600°C [25]. This high temperature exhaust gas can be used in a heat recovery steam generator (HRSG) to produce the steam for a steam turbine cycle. The efficiency of the combined cycle is higher than the efficiency of either of the cycles when they are operated individually. The main application of combined cycle plants is base-load generation of electricity [25].

A schematic of a combined cycle is shown in Figure 2.1. The combined cycle consists of a gas turbine cycle which in itself contains a compressor, combustion chamber and turbine. The inlet stream to the compressor is ambient air which the compressor compresses to a pressure typically in the range of 15 to 35 bar. The high pressure air then goes to the combustion chamber where the fuel is then combusted. The temperature of the gas that leaves the combustion chamber and enters the turbine is in the range of 1100°C to as high as 1500°C. The high temperature and pressurized flue gas is then expanded through the turbine. Next, the flue gas goes to the HRSG which acts as the boiler for the steam cycle. After the gas goes through the HRSG it is exhausted into the atmosphere. The steam cycle consists of the HRSG, the steam turbine, and a condenser. The HRSG shown in Figure 2.1 produces steam at two pressure levels. The HRSG studied here consists of two steam drums, two economizers that heat up the water, two evaporators that produce steam, and two superheaters that increase the temperature of the steam.

An example of a combined cycle power plant that has a two pressure level steam cycle is the Monterrey power plant in Mexico [14]. The cycle consists of a 160 MW gas turbine and a 90 MW steam turbine unit. The pressure ratio for the gas turbine is around 32 and the ISO turbine inlet mixed temperature is 1255°C and the exhaust temperature is 650°C. The HRSG generates high pressure steam with a pressure of 160 bar and a temperature of 565°C. The low pressure steam has a pressure of 7 bar and a temperature of 320°C. The condenser at this power plant is an air cooled condenser that operates at an air temperature of 30°C. The efficiency of the plant is around 54%. Siemens reported in 2011 that the combined cycle power plant Irsching 4 in Germany reached an efficiency of 60.75%, with an output of 578 MW, which is the current world record [28].

2.3 Oxy-fuel Combined Cycles

Oxy-fuel combined cycles represent a means to implement carbon capture on combined cycles. The basic principle of oxy-fuel combustion was introduced in chapter 1.1.3. The two oxy-fuel combustion combined cycles that are studied in this thesis are the Graz cycle and the Semi Closed Oxy-fuel Combustion Combined Cycle (SCOC-CC). The cycles that are studied are in the mid-size range, which means that the net power output from the cycles is typically around 100 MW.

2.3.1 Air Seperation Units

Different methods, such as cryogenic distillation, adsorption using multi-bed pressure swing units, and polymeric membranes are available to separate oxygen from air [5]. The only technology that has reached a mature technology level is cryogenic distillation. Cryogenic distillation plants are used today in plants that can produce up to 3000 tonnes of O_2 per day [3].

The first step in the cryogenic process is to remove unwanted particles from the air, either by filters or they are chemically absorbed of surfaces. The next step is to compress the air. After compression the air is cooled down to a temperature which is below the boiling point of oxygen. A separation column is used to separate the air into its components. Since nitrogen has a lower boiling temperature than oxygen, and the separation column has a temperature that is higher than that temperature but lower than the boiling temperature of oxygen, the oxygen will be in liquid form but the nitrogen will be in a gaseous state. The gaseous nitrogen will collect at the top and liquid oxygen will stay at the bottom of the column.

The design and simulation of the air separation unit is outside the scope of the current thesis. Instead a constant energy per mass flow of oxygen has been assumed to be 900 kJ/kg O_2 for the production of oxygen which has a pressure of 2.38 bar and a composition of 95% O_2, 3% Ar and 2% N_2 per mass. The energy to compress the oxygen up to the pressure which is in the combustion chamber is assumed to be 325 kJ/kg O_2. These values come from a study conducted by Graz university in 2005, and are estimates that were established in cooperation between engineers from Statoil and researchers from Graz University [24].

2.3.2 SCOC-CC

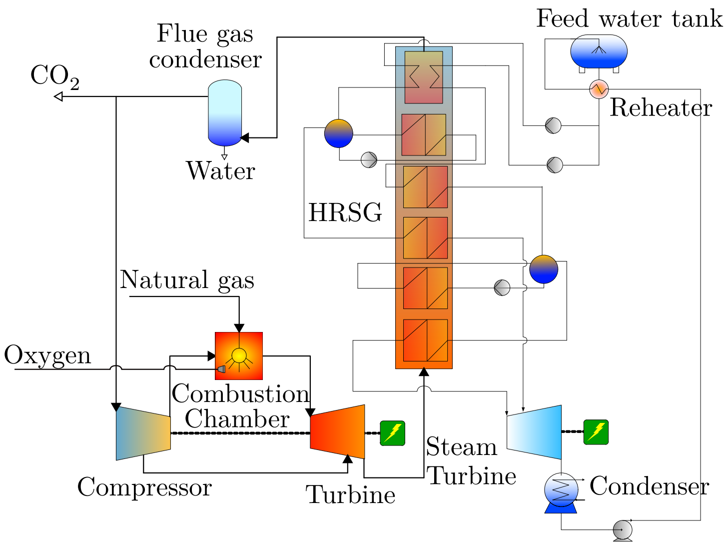

Figure 2.2: *Schematic of the SCOC-CC.*

The main layout of the SOCC-CC, which is shown in Figure 2.2, is similar to the conventional combined cycle. The main difference is that the combustion takes place with pure oxygen instead of air. This means that the major products after the combustion are CO_2 and H_2O. The combustion products leave the combustion chamber with a temperature of 1400°C. The hot gases are then expanded in the turbine and leave the turbine with a temperature of 620°C and a pressure of around 1 bar. The cooling flow for the turbine blades is taken from the compressor. The energy left in the flue gas is then used in the HRSG to produce the steam for the bottom cycle. The flue gas leaves the HRSG with a temperature of 69°C which is lower than in a regular dual-pressure combined cycle. The reason that the temperature is lower for the SCOC-CC is that the specific heat of the flue gas is lower than in a conventional combined plant. After the HRSG the flue gas goes through a condenser where water is condensed from the flue gas. The condenser uses water as cooling media with a temperature of 15°C to remove the water from the flue gas. The flue gas contains mainly carbon dioxide after the condenser. A major part of the carbon dioxide stream, 93%, goes back to the compressor while the rest goes to the CO_2 compression and is then transported to storage. The compressor raises the pressure to 37 bar and the exit temperature from the compressor is around 394°C. The composition of the working fluid at different locations is shown in Table 2.1.

The bottoming cycle is in principle aspects the same cycle as in the normal combined

Table 2.1: *Composition of the working media in the SCOC-CC.*

	Composition [%]					R
	Ar	CO_2	H_2O	N_2	O_2	$\left[\frac{J}{kg\ K}\right]$
Compressor	4.06	92.0	0.98	2.86	0.12	195.5
Turb. inlet	3.82	86.5	6.91	2.68	0.11	211.5
Turb. exit	3.87	87.7	5.55	2.72	0.11	207.8

cycle. It consists of a HRSG, steam turbines, a condenser, pump, and a deaerator. The units in the HRSG are the low pressure heat exchangers and the high pressure heat exchangers. The low pressure heat exchangers are the reheater, the economizer, the evaporator, and the superheater. The high pressure heat exchangers are the economizer, the evaporator, and the superheater. The HRSG delivers high pressure steam with a pressure of 127 bar and a temperature of 565°C. The pressure of the low pressure steam is close to 10 bar and the steam has a temperature of 210°C. Figure 2.3 shows the temperature and the energy transfer between the flue gas and the steam. The turbines expand the steam to a pressure of 0.034 bar and a temperature of 26°C. It is assumed that the cooling water for the condenser has a temperature of 15°C.

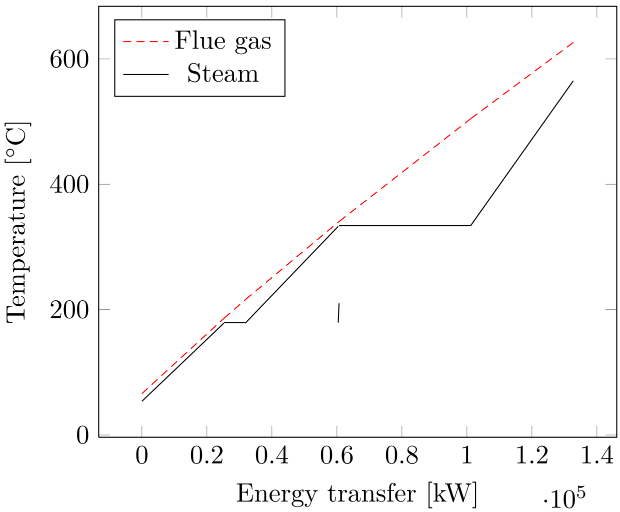

Figure 2.3: *Temperature vs. the energy transfer for the HRSG in the SCOC-CC.*

2.3.3 Graz Cycle

The Graz cycle is another concept that uses oxy-fuel in a combined cycle. An schematic of the Graz cycle is shown in Figure 2.4. The Graz cycle consists of a topping cycle and uses two bottoming cycles. The topping cycle of the Graz cycle also consists of a compressor,

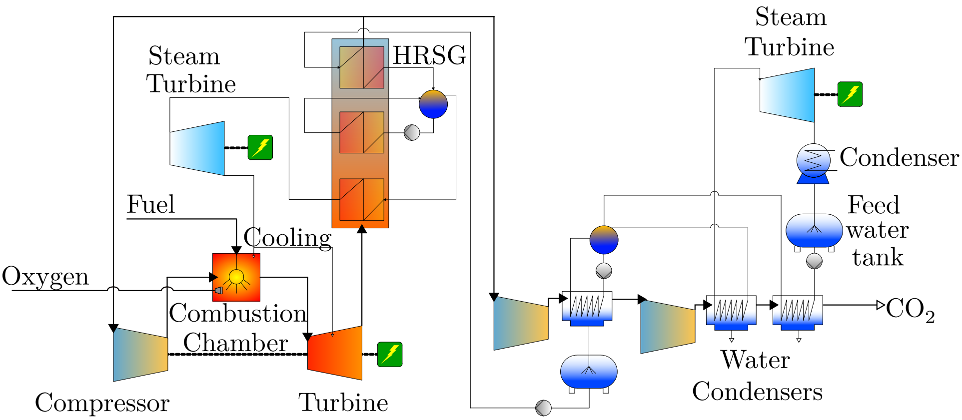

Figure 2.4: *Schematic of the Graz cycle.*

Table 2.2: *Composition of the working media in the Graz cycle.*

	Composition [%]					R
	Ar	CO_2	H_2O	N_2	O_2	$\left[\frac{J}{kg\ K}\right]$
Compressor	1.55	20.9	77.4	0.03	0.13	400.2
Turb. inlet	1.74	23.6	74.5	0.04	0.15	392.3

combustion chamber and a turbine. The difference for the topping cycle in the Graz cycle compared to SCOC-CC is the working media which consists of a higher fraction of steam in the Graz cycle. The composition of the working media for the Graz cycle is shown in Table 2.2.

The temperature of the gas leaving the combustion chamber is 1400°C and the pressure is 47.4 bar. The gas expands in the turbine to a pressure of 1.06 bar with a temperature of 572°C. The energy left in the flue gas is then used in the HRSG to generate steam for the first bottoming cycle. The flue gas leaves the HRSG with a temperature of 125°C. The temperature of the flue gas is limited because the gas contains water, which should not be condensed before the gas enters the compressor. Half of the flue gas is sent to the compressor, while the other half goes to the condensers. The compressor, as stated before, raises the pressure to 47.4 bar which results in a temperature of 710°C. This temperature is too high for the blade material in the compressor and it suggests the need to use intercooling in the compressor.

The HRSG in the Graz cycle consists of only one pressure level. The HRSG consists of an economizer, an evaporator, and a superheater. The steam produced in the HRSG has a pressure of 140 bar and a temperature of 401°C. Figure 2.5 shows the temperature and the energy transfer between the flue gas and the steam. The steam is then expanded in a turbine to a pressure of 47.4 bar and a temperature of 261°C. This steam is then used to cool both the combustion chamber and the gas turbine blades. The water used in the first bottoming cycle is water that is condensed from the flue gas.

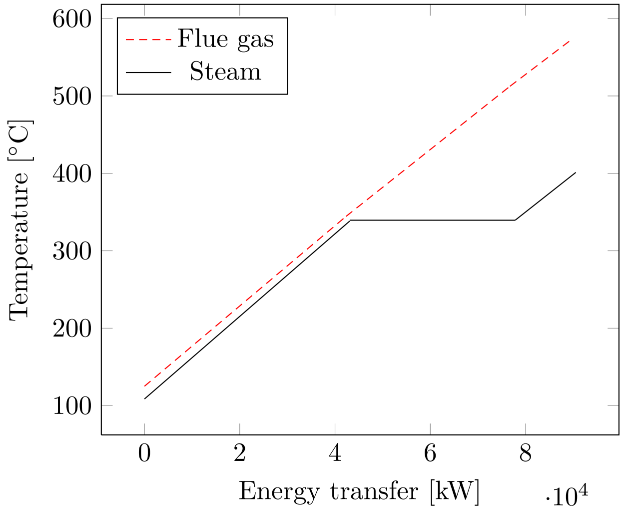

Figure 2.5: *Temperature vs. the energy transfer for the HRSG in the Graz cycle.*

The second bottoming cycle uses the heat produced when the water is condensed from the flue gas. The cycle is operating at sub-atmospheric pressure. The pressure of the steam is 0.73 bar and has a temperature of 134°C. The steam is expanded to 0.025 bar with a temperature of 21°C.

3 Conceptual Compressor Design

The purpose of the compressor is to increase the pressure of the working fluid. An axial compressor consists of stages which contain two blade rows. The blades in the first row rotate, and are called rotors while the blades in the second row are stationary and are either called stators or nozzles. In both rows, the blades slow down the local relative flow velocity and in such behave like diffusers. The deceleration possible is limited, since if the flow is slowed down too much, it will separate from the blades and the compressor is likely to exhibit flow instabilities called stall or surge. The flow in the compressor is unsteady, three dimensional and viscous effects influence the flow in an intricate manner.

Compressor design is an iterative process using a number of tools that come from the arsenal of engineering, such as thermodynamics, fluid dynamics, solid mechanics, manufacturing, material mechanics and structural mechanics. The conceptual design of a compressor starts with one dimensional thermo-fluid design, called mean-line design. Thereafter a two-dimensional design approach based on inviscid flow and correlation based loss predictions called throughflow is frequently applied. The next step is to go to detailed three dimensional design, using advanced computational fluid dynamics codes. Along with the aerodynamic design, structural dynamics and solid mechanics modelling have to be performed before compressor rig design and tests can commence. To achieve a good solution for the compressor design there is often a need to iterate between the design stages described above. Even after the testing phase of the compressor has been initiated modifications to the designs are often needed to ensure efficient and reliable operation in the entire working range.

3.1 One Dimensional Design

One dimensional design methods simplifies the flow, and assumes that it is steady and inviscid, by considering only the variation in the flow along the mean radius through the compressor. The method neglects spanwise variations and uses parameters that represent average conditions. The flow field in a compressor is a complex three dimensional system which can be modelled using computational fluid dynamics. Still, the one dimensional method provides a necessary starting point for the design based on a limited number of input parameters. It also provides a rapid convergence which can be used to explore a wide range of different compressor designs.

3.1.1 Mean-line Code

The one dimensional model is used to predict the flow at the mean radius, shown in Figure 3.1. A design process based on such a simplified model is called a mean-line design. The mean-line code is based on solving the mean velocity triangles, shown in Figure 3.2, and using the Euler equation, Equation 3.1, to relate the enthalpy change to the velocity triangle.

$$\dot{W}_x = \dot{m}\Delta H = \dot{m}(U_2 c_{\theta_2} - U_1 c_{\theta_1}) \tag{3.1}$$

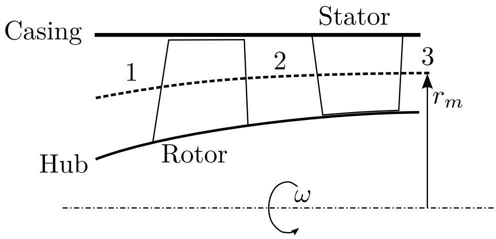

Figure 3.1: *Meridional view of compressor stage.*

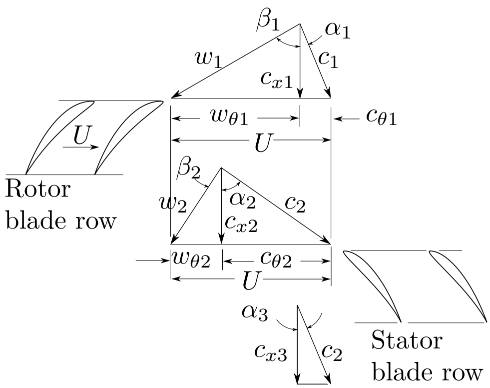

Figure 3.2: *Velocity diagram for a compressor stage.*

To take viscous effects into account as part of the mean-line design, correlations are used. The correlations found in open literature for blade and endwall losses are generally based on traditional blade profile types such as double circular arc (DCA), or NACA. The mean-line code used herein assumes that the blades are DCA blades.

The parameters for the boundary conditions are the mass flow, the inlet temperature and pressure, and the working fluid in the compressor. The values for these parameters are received from the cycle simulation tool. Other input parameters are number of stages, rotational speed, relative tip Mach number at the rotor of the first stage, axial inlet Mach number, stage loading (Equation 3.2), degree of reaction (Equation 3.3), aspect ratio of the blades, the geometry of each stage such as constant hub radius, constant mean radius, or constant casing radius, the ratio of the clearance between the blade and the casing and the blade chords.

$$\psi = \frac{\Delta H}{U^2} \tag{3.2}$$

$$R = \frac{\text{static enthalpy rise in the rotor}}{\text{static enthalpy rise in the stage}} \tag{3.3}$$

Some of the parameters will be used in connection to numerical procedures to optimize the compressor design. These parameters are the number of stages, stage loading, degree of reaction, and geometry. Other parameters, i.e the relative tip Mach number, the axial inlet Mach number, the aspect ratio, and the ratio of clearance over chord, are selected based on available empirical data and past design experience.

An interesting example of how empirical data has improved the design of compressors is the aspect ratio of the blades. Before the 1960s there was a trend to use blades with high aspect ratios. This was mainly due to the requirement of having short compressors. What changed the trend, from high aspect ratio, to low, was not the result of an increasing understanding of the mechanism of the flow but empirical evidence from different designs [6]. The evidence showed that blades with low aspect ratios can handle higher stage loading and the compressor will have higher stall margin.

3.1.2 Empirical Models

Here the empirical models used in the mean-line code will be introduced. The nomenclature for cascades used in the models, is shown in Figure 3.3.

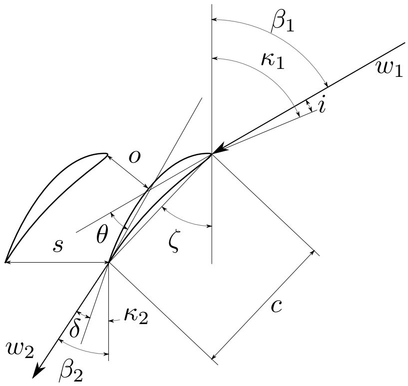

Figure 3.3: *Nomenclature for cascade.*

McKenzie [16]

Mckenzie noticed that for 50% reaction designs the blade stagger angle (ζ), appeared to determine the flow coefficient for the maximum stage efficiency. This was interpreted as a relationship between the stagger angle and vector mean flow angle β_m. The relationship was found to be relative independent of the reaction. The relationship is expressed by Equation 3.4 where $\tan\beta_m = 0.5(\tan\beta_1 + \tan\beta_2)$ by definition.

$$\tan\beta_m = \tan\zeta + 0.213 \tag{3.4}$$

McKenzie proposed an alternative design rule for blades with low stagger angle since it was noticed that the peak efficiency for compressors that have blades with low stagger angle occurs close to stall. Equation 3.5 gives the new design rule that provides larger stall margin for the compressor.

$$\tan\beta_m = \tan\zeta + 0.15 \tag{3.5}$$

The camber angle can be computed, since the blades are double circular arc blades, using the inlet flow angle and the stagger angle

$$\theta = 2(\beta_1 - \zeta)\,. \tag{3.6}$$

Wright and Miller [34]

The first part in the profile loss model uses a correlation to calculate the equivalent diffusion ratio from the aerodynamic inlet and exit conditions, blade spacing to chord ratio, and the thickness to chord ratio

$$D_{eq} = \left\{1 - \frac{w_2}{w_1} + \left[0.1 + \frac{t}{c}\left(10.116 - 34.15\frac{t}{c}\right)\right]\frac{s}{c}\frac{w_{\theta 1} - w_{\theta 2}}{w_1}\right\}\frac{w_1}{w_2} + 1.0\,. \tag{3.7}$$

The second part in the profile loss model relates the Lieblein loss parameter to the equivalent diffusion ratio and inlet Mach number as shown Figure 3.4. The definition of

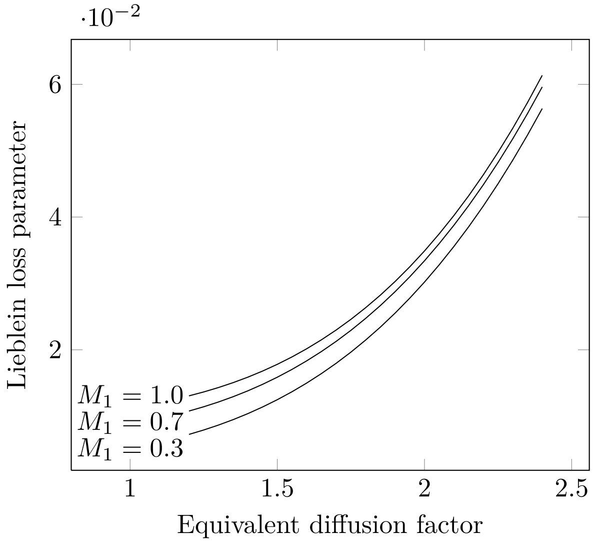

Figure 3.4: *Correlation for profile loss coefficient [34].*

the Lieblein loss parameter is

$$0.5\omega_p\left(\frac{w_1}{w_2}\right)^2\cos\beta_2\,. \tag{3.8}$$

Since the model assumes that the Reynolds number is 10^6, it needs to be adjusted for the effect of Reynolds number.

The model for endwall losses comes from the observed trends that as tip clearance increases the total loss increases, while the maximum achievable loading decreases. It was also observed that the maximum achievable loading decreases with increasing aspect ratio. The correlation that is presented in [34] is

$$\omega_{ew}\frac{h}{c}\frac{w_1^2}{w_2^2} = \text{func}(\frac{\varepsilon}{c}, \text{loading}) \tag{3.9}$$

where the loading in the correlation is expressed as the diffusion factor, which is computed with Equation 3.10.

$$DF = 1 - \frac{w_2}{w_1} + 0.5\frac{s}{c}\frac{w_{\theta 1} - w_{\theta 2}}{w_1} \tag{3.10}$$

The correlation for the endwall loss parameter is shown in Figure 3.5.

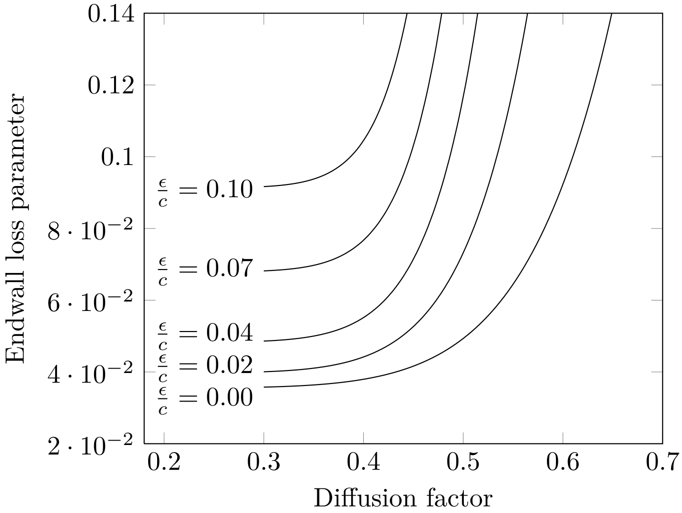

Figure 3.5: *Correlation for endwall loss coefficient [34].*

As mentioned for the profile loss a correction is needed for the Reynolds number. The same correction is also needed for the endwall loss. The correction assumes that the change in loss with Reynolds number in the laminar region follows the Blasius power law for the effect of Reynolds number on the drag of a flat plate. In the region where the Reynolds number is between 10^5 and 10^6 the change in loss with Reynolds number is resembling the Prandtl equation for the skin friction of a flat plate in a hydraulically smooth turbulent flow. When the flow is fully turbulent it is assumed to be hydraulically rough and there are no effects from the Reynolds number. The losses are then assumed to be constant. The correction factors are expressed in Equation 3.11 and shown in Figure 3.6.

$$\frac{\omega}{\omega_{Re=10^6}} = \begin{cases} 489.8Re^{-0.5} & \text{if } Re < 10^5 \\ 13.8Re^{-0.19} & \text{if } 10^5 < Re < 10^6 \\ 1.0 & \text{if } Re > 10^6 \end{cases} \tag{3.11}$$

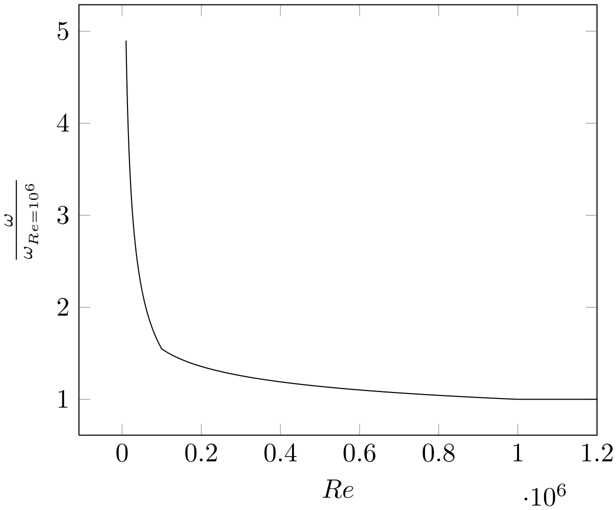

Figure 3.6: *Reynolds number*

The correlation for minimum loss incidence that Wright and Miller derived, relates the minimum loss incidence to the ratio of throat width to inlet spacing and the inlet Mach number.

$$\frac{o}{s \cos \beta_{1ml}} = 0.155 M_1 + 0.935 \tag{3.12}$$

The correlation proposed by Wright and Miller to calculate the deviation angle is a modified form of the Carter's rule. Carter's rule states that the deviation angle is a function of the camber angle and the space chord ratio ($\delta = m\theta\sqrt{\frac{s}{c}}$). The new correlation is

$$\delta = 1.13m \left(\theta \sqrt{\frac{s}{c}} + 3.0 \right) + 1.0 \left(1 - \frac{c_{x2}}{c_{x1}} \right) \tag{3.13}$$

where the correlation for the coefficient m, is shown in Figure 3.7.

Schwenk [27]

The shocks encountered in transonic compressor rotors consists of a bow shock and a passage shock. Operation conditions control the shape and location of the shocks. Schwenk proposed a model to estimate the passage shock losses at maximum compressor efficiency. The model calculates the average of the peak suction surface and the relative inlet Mach number. The Prandtl-Meyer expansion equations were used to compute the peak suction surface Mach number.

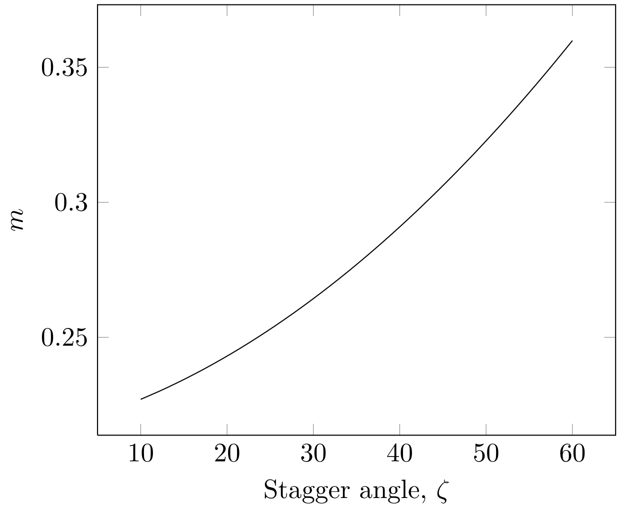

Figure 3.7: *Coefficient for camber and space/chord ratio. [34].*

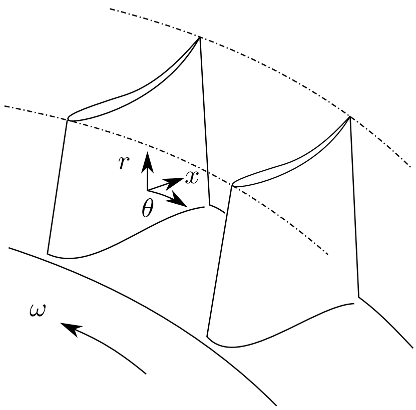

Figure 3.8: *Coordinate system.*

3.2 Two Dimensional Design

3.2.1 Streamline Curvature Method

The streamline curvature approach solves the governing equations in the meridional plane, see Figure 3.9, the blade to blade plane, or computes a coupled solution of these. However, most practical approaches solve the equations in the meridional plane. The assumptions made when using the streamline curvature approach are that the flow is steady, adiabatic, axisymmetric, inviscid, and with negligible body forces. The governing equations are the continuity equation

$$\frac{\partial(\rho c_r)}{\partial r} + \frac{\partial(\rho c_x)}{\partial x} = 0\,, \tag{3.14}$$

the momentum equation in axial direction

$$c_r \frac{\partial c_x}{\partial r} + c_x \frac{\partial c_x}{\partial x} = -\frac{1}{\rho}\frac{\partial p}{\partial x}\,, \tag{3.15}$$

the momentum equation in radial direction

$$c_r \frac{\partial c_r}{\partial r} + c_x \frac{\partial c_r}{\partial x} - \frac{c_\theta^2}{r} = -\frac{1}{\rho}\frac{\partial p}{\partial r}\,, \tag{3.16}$$

and the momentum equation in tangential/circumferential direction

$$c_r \frac{\partial V_\theta}{\partial r} + c_x \frac{\partial c_\theta}{\partial x} - \frac{c_r c_\theta}{r} = 0\,. \tag{3.17}$$

The streamlines and computational stations for the method are shown in Figure 3.9. The streamline curvature method solves the governing equations by first rewriting the

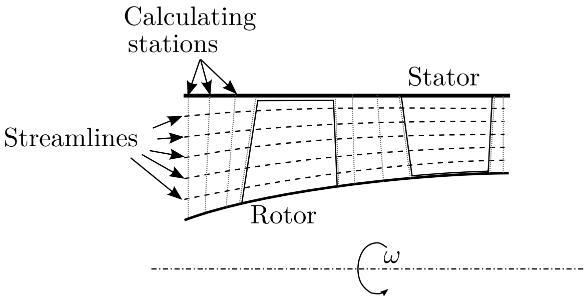

Figure 3.9: *Streamline curvatures in a compressors stage (meridional plane).*

equations into equations for angular momentum, entropy, and radial equilibrium. The method solves the equations using an iterative procedure while satisfying the overall continuity equation. A more detailed description of the streamline curvature method can be found in e.g. [6].

The approach used in the thesis is to use a commercial program that implements the streamline curvature method [26]. The program SC90C is developed by PCA engineers [26]. The program uses Wright and Miller for loss and deviation correlations, the same models as is used in the mean-line design program. The code also incorporates the spanwise mixing scheme from Gallimore [8, 9]. The spanwise mixing is modelled as a turbulent diffusion process. The process redistributes the losses across the span, and by doing so reduce the apparent losses near the endwalls by spreading the losses toward the midheight.

An important design criteria for compressors is stability assessment. Compressor surge is an instability where the flow reverses and recovers at a frequency of a few cycles per

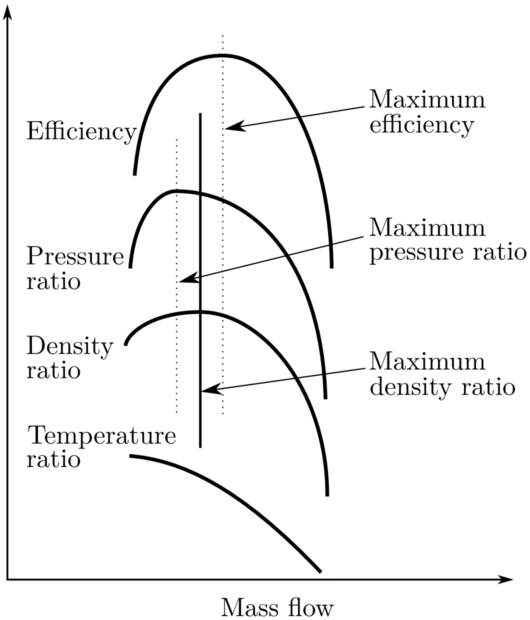

Figure 3.10: *Relative flows for maximum efficiency, pressure and density ratios [16].*

second. An idea proposed by McKenzie [16] for surge is that the maximum density ratio is the determining parameter for surge onset rather than the maximum pressure ratio. Figure 3.10 shows typical temperature ratio, efficiency, and pressure ratio curves as a function of mass flow when the rotation speed is held constant. It is shown in the figure that the pressure ratio is lower when the maximum efficiency occurs and the mass flow higher.

The model built on this explanation assumes that surge will be encountered when the density ratio reached the maximum. This model is easy to implement and tends to be more conservative than most other surge predictions. Miller and Wasdell showed that this method was in fairly good agreement to surge measurements [18].

3.3 Optimization

To reach a satisfying compressor design a number of contradicting requirements need to be fulfilled. These requirements are e.g. high efficiency, wide operating range, high total pressure ratio per stage, low weight, and high durability [19]. The compressor design is therefore a multi-objective design problem.

The difference between a single objective optimization problem and a multi-objective formulation is that single objective problems have a unique solution, while the multi-objective have a set of compromised solutions. These are known as trade-off surfaces, Pareto optimal solutions or non-dominated solutions [20]. The meaning of these trade-off solutions is that if all objectives are considered then no other solutions in the search space are superior to them.

A solution to a multi-objective optimization is comprised by a number of solutions, all optimal for a particular trade between the objectives. It is therefore possible to transform the problem to a series of single objective problems with a fixed trade between the objectives. The advantage of a multi-objective solver is that it can use information from all the trade combinations simultaneously and provide a more efficient solution process.

The goal of the multi-objective optimization is to reveal the trade-off information between different objectives by finding as many Pareto optimal solutions as possible. A class of optimization methods that is particularity well suited for multi-objective formulations are evolutionary algorithms. The evolutionary algorithms are based on adaptive search techniques and it mimics Darwins's theory of survival of the fittest [32]. Most often the process starts from a randomly selected first generation. These are the initial values for the parameters used in the optimization scheme. The algorithm will then run the simulation and after that select the next generation based on the fitness of the generation, which is selected according to the objective function values. This optimization process is the same mechanism that the natural evolution process uses, i.e. inheritance, mutation, selection, and crossover.

As part of this work a multi-objective optimization environment has been set up. A one-dimensional compressor design code is used to establish a first guess on a design. An analytic mapping is then used to produce a first guess on the blade angles for a througflow solver. The throghflow solver is then interfaced with a software, iSIGHT [10], which allows multi-objective optimization. The work is described in more detail in [30].

4 Summary of Papers

4.1 Paper A: Conceptual Design of a Mid-Sized, Semi-closed oxy-fuel combustion combined cycle

Paper A presents a conceptual design study of a semi-closed oxy-fuel combustion combined cycle. The cycle studied had a net power output of 100 MW, which is classified as a cycle in the mid-size range of the power output. The sizes of cycles that have been studied previously, have concentrated on plants intended for the large power output range. The study focused on the simulation of the cycle, using the cycle simulation tool described in Section 2.1 and on the conceptual design of the gas turbine. The compressor was designed using the mean-line design tool described in Section 3.1.1, and the conceptual design of the turbine was accomplished using the conceptual mean-line design program LUAX-T. The configuration selected for the gas turbine was a single-shaft design, where the motivation behind the selection is the simplicity of gas turbine.

The study resulted in a cycle efficiency of 47%. By considering constraints of the compressor first stage and the turbine last stage, a rotational speed of 5200 rpm was selected. For this selection an 18-stage compressor and a four stage turbine was designed.

The author and Tomas Grönstedt designed the compressor and wrote the compressor section in the paper. The author also programmed the link between IPSEpro and REFPROP. The cycle simulation and the conceptual design of the turbine were performed by Majed Sammak and Magnus Genrup. Klas Jonshagen developed components used in the cycle simulation program and Marcus Thern assisted in developing the real gas calculations.

4.2 Paper B: Multicriteria Optimization of Conceptual Compressor Aerodynamic Design

Paper B describes a design method that incorporates one dimensional and two dimensional design tools and an optimization environment. The design method aims to maximize the efficiency of the compressor while simultaneously taking into account the stability of the compressor through the predicted surge margin. The first step in the design method is to use the one dimensional code which is a mean-line design tool, to compute the boundary conditions for the two dimensional code. This is accomplished by using a simplified solution to the radial equilibrium equation to map the one dimensional results onto two dimensions so the results can be used as the boundary conditions for the two dimensional design code. The optimization algorithm updates the boundary conditions so that an optimal compressor design is established.

The method is used in a case study, where a compressor is designed for an open rotor engine configuration intended for aircraft propulsion. At the time of this work the throughflow code was not able to work with the gas mixtures present in the oxy-fuel cycles. Furthermore, a license was only available at Volvo Aero. It was therefore decided to start developing the framework for an air breathing compressor. Through an agreement with the company developing the code [26], Chalmers has obtained the source code to provide an updated version that can handle the gas mixtures present in the oxy-fuel cycles.

The case study resulted in multiple designs that produced a Pareto front of design solutions. This means that the designs are optimal in that sense that to increase either of the objective functions, efficiency or stability, the other objective function is compromised. The value generated by this work was primarily to establish the optimization environment. This will allow future work applied to the Graz and SCOC-CC compressors.

4.3 Paper C: Single and Twin-Shaft Oxy-Fuel Gas Turbine Design in a Mid-Size Semi-Closed Oxy-Fuel Combustion Combined Cycle

Paper C compares two different layouts, single- and twin-shaft, of the gas turbine for the SCOC-CC. The paper describes the turbomachinery preliminary mean-line design of the compressor and turbine. The conceptual turbine design was performed using the mean-line design code LUAX-T, while the conceptual compressor design was accomplished using the mean-line design code described in Section 3.1.1.

The cycle simulation resulted in a cycle performance of 46% net efficiency, and a net output of 106 MW. The design of the single-shaft gas turbine was reported in paper A. The conceptual design of the twin-shaft gas turbine resulted in a rotational speed of 7200 rpm for the gas generation turbine, and 4500 rpm for the power turbine. The gas generation turbine, which powers the compressor, was designed with two stages, while the design of the power turbine resulted in three stages. The conceptual design of the compressor resulted in a compressor with 14 stages. From the results of this study it was concluded that both single- and twin-shaft oxy-fuel gas turbines have advantages. The choice of a twin-shaft gas turbine can be motivated by the smaller compressor size and the advantage of greater flexibility in operation, mainly in off-design mode. However, the advantages of a twin-shaft design must be weighed against the inherent simplicity and low cost of the simple single-shaft design.

The author was responsible for the conceptual design of the compressors and wrote the compressor part of the paper. The cycle simulation and the conceptual design of the turbine were performed by Majed Sammak and Magnus Genrup.

4.4 Paper D: A Comparative Analysis of Two Competing Mid-Size Oxy-Fuel Combustion Cycles

Paper D reports a study where two mid-sized oxy-fuel combustion combined cycles are compared. The two cycles are the Semi-closed Oxy-fuel Combustion Combined Cycle and the Graz cycle, which are described in Sections 2.3.2 and 2.3.3 respectively. The cycles are simulated using the simulation tool described in Section 2.1. The cycle modelling and simulation of the Graz cycle was performed by the author while for the SCOC-CC it was carried out by Majed Sammak.

The compressor design was accomplished using the mean-line design tool described in Section 3.1.1. The turbine design was established using the LUAX-T code from Lund University and the work was done by Majed Sammak and Magnus Genrup.

The main result of the study is that the Graz cycle is expected to achieve around 3% higher net efficiency than the SCOC-CC. The configuration used in the SCOC-CC was to have a two-shaft configuration and in the Graz cycle it was decided to have a geared configuration of the compressor and two turbines, one that runs the compressor and one that runs the generator. The design of the compressor for the SCOC-CC was optimized and it was concluded that a compressor with 14 stages had a reasonably high efficiency. The conceptual design of the gas turbine for the Graz cycle resulted in a low pressure and a high pressure compressor that both have six stages. The design of the turbine part resulted in a high pressure turbine with 3 stages and a low pressure turbine that has 4 stages.

References

[1] International Energy Agency. *CO_2 emissions from fuel combustion - highlights*. International Energy Agency, 2011. URL: www.iea.org/co2highlights.

[2] International Energy Agency. *IEA Press Releases*. 2011. URL: http://www.iea.org/press/pressdetail.asp?PRESS_REL_ID=429.

[3] RJ Allam, V. White, N. Ivens, and M. Simmonds. The oxyfuel baseline: revamping heaters and boilers to oxyfiring by cryogenic air separation and flue gas recycle. *Carbon dioxide capture for storage in deep geologic formations* **1** (2005), 451–475.

[4] Y.A. Çengel and M.A. Boles. *Thermodynamics: an engineering approach*. Fourth ed.

[5] John Conti, Paul Holtberg, Linda E. Doman, Kay A. Smith, James O'Sullivan, Kenneth R. Vincent, Justine L. Barden, Phyllis D. Martin, Justine Barden, Philip Budzik, et al. *International Energy Outlook 2011*. 2011, U.S. Energy Information Administration.

[6] N. A. Cumpsty. *Compressor Aerodynamics*. Longman Scientific & Technical, Longman Group UK, Limited Essex CM20 2JE, England, co-published in the United States with John Wiley & Sons, Inc, 1989. ISBN: 0470213345.

[7] European Environment Agency. *Greenhouse gas emission trends and projections in Europe 2008*. European Environment Agency, 2008. URL: www.eea.europa.eu/publications/eea_report_2008_5.

[8] SJ Gallimore. Spanwise Mixing in Multistage Axial Flow Compressors. Part II - Throughflow Calculations Including Mixing. *Journal of Turbomachinery* **108** (1986), 10.

[9] M. A. Howard and S. J. Gallimore. Viscous throughflow modeling for multistage compressor design. *Journal of turbomachinery* **115** (1993), 296.

[10] *Isight User's Guide, Version 5.0*. Engineous Software, Inc., Cary, NC, USA. 2010.

[11] K. Jonshagen. "MODERN THERMAL POWER PLANTS. Aspects on Modelling and Evaluation". PhD thesis. Department of Heat and Power Engineering, Lund university, 2011.

[12] K. Jordal. "Modeling and Performance of gas turbine cycles with various means of blade cooling". PhD thesis. Department of Heat and Power Engineering, Lund university, 2001.

[13] M. Kanniche, R. Gros-Bonnivard, P. Jaud, J. Valle-Marcos, J.M. Amann, and C. Bouallou. Pre-combustion, post-combustion and oxy-combustion in thermal power plant for CO_2 capture. *Applied Thermal Engineering* **30**.1 (2010), 53–62.

[14] R. Kehlhofer, B. Rukes, F. Hannemann, and F. Stirnimann. *Combined-cycle gas & steam turbine power plants*. Pennwell Books, 2009.

[15] EW Lemmon, MO McLinden, and ML Huber. REFPROP: reference fluid thermodynamic and transport properties. *NIST Standard Reference Database* **23** (2007).

[16] A. B. McKenzie. *Axial Flow Fans and Compressors: Aerodynamic Design and Performance*. Cranfield Series on Turbomachinery Technology, 1997 (Ashgate Publishing Limited).

[17] B. Metz, Ogunlade Davidson, Heleen de Coninck, Manuela Loos, and Leo . Meyer, eds. *IPCC special report on carbon dioxide capture and storage*. Cambridge University Press, 2005.

[18] DC Miller and DL Wasdell. Off-design prediction of compressor blade losses. *C279/87, pgs* (1987), 249–258.

[19] S. Obayashi, D. Sasaki, and A. Oyama. Finding tradeoffs by using multiobjective optimization algorithms. *Transactions of the Japan Society for Aeronautical and Space Sciences* **47**.155 (2004), 51–58. ISSN: 0549-3811.

[20] A. Oyama and M.S. Liou. Multiobjective optimization of a multi-stage compressor using evolutionary algorithm. *AIAA Paper* **3545** (2002).

[21] M.C. Romano, P. Chiesa, and G. Lozza. Pre-combustion CO_2 capture from natural gas power plants, with ATR and MDEA processes. *International Journal of Greenhouse Gas Control* **4**.5 (2010), 785–797.

[22] M. Sammak, M. Genrup, E. Thorbergsson, and T. Grönstedt. Single and Twin-Shaft Oxy-Fuel Gas Turbine Design in a Mid-Size Semi-Closed Oxy-Fuel Combustion Combined Cycle. *ASME Turbo Expo 2012: Power for Land, Sea and Air, 11-15 June* (2012).

[23] M. Sammak, K. Jonshagen, M. Thern, M. Genrup, E. Thorbergsson, and T. Grönstedt. Conceptual Design of a Mid-Sized, Semi-closed oxy-fuel combustion combined cycle. *ASME Turbo Expo 2011: Power for Land, Sea and Air, 6-10 June* (2011).

[24] W. Sanz, H. Jericha, F. Luckel, E. Göttlich, and F. Heitmeir. A Further Step Towards a Graz Cycle Power Plant for CO2 Capture. *ASME Paper GT2005-68456, ASME Turbo Expo* (2005).

[25] H.I.H. Saravanamuttoo, G.F.C. Rogers, H. Cohen, and P.V. Straznicky. *Gas turbine theory*. Sixth ed. Pearson Education, 2009.

[26] *SC90C - A streamline curvature program for axial compressors, Userguide*. PCA Engineers Ltd, Nettleham, Lincoln, UK. 2008.

[27] F.C. Schwenk, G.W. Lewis, and M.J. Hartmann. *A preliminary analysis of the magnitude of shock losses in transonic compressors*. NASA RM E57A30, 1957.

[28] Siemens. *Trail-blazing power plant technology*. `http://www.siemens.com/press/en/pressrelease/?press=/en/pressrelease/2011/fossil_power_generation/efp201105064.htm`. Retreived February, 2012.

[29] SimTech Simulation Technology. User Documentation: Program Modules and Model Libraries. *IPSEpro Process Simulator* (2003).

[30] Egill Thorbergsson and Tomas Grönstedt. Multicriteria Optimization of Conceptual Compressor Aerodynamic Design. *20th International Society for Airbreathing Engines* (2011).

[31] Egill Thorbergsson, Tomas Grönstedt, Majed Sammak, and Magnus Genrup. A Comparative Analysis of Two Competing Mid-Size Oxy-Fuel Combustion Cycles. *ASME Turbo Expo 2012: Power for Land, Sea and Air, 11-15 June* (2012).

[32] S. Tiwari, P. Koch, G. Fadel, and K. Deb. “AMGA: an archive-based micro genetic algorithm for multi-objective optimization”. *Proceedings of the 10th annual conference on Genetic and evolutionary computation*. ACM. 2008, pp. 729–736.

[33] W. Wagner and A. Kruse. *Properties of water and steam: the industrial standard IAPWS-IF97 for the thermodynamic properties and supplementary equations for other properties: tables based on these equations*. Springer-Verlag, 1998.

[34] PI Wright and DC Miller. An improved compressor performance prediction model (1992).

A Derivation of the Radial Equilibrium Equation

The geometry and the nomenclature are shown in Figure A.1. The momentum equation

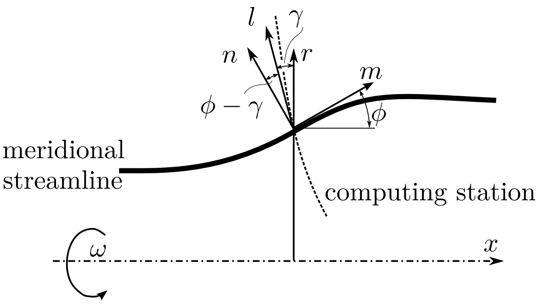

Figure A.1: *Coordinate directions in the meridional plane.*

in meridional direction is

$$c_m \frac{\partial c_m}{\partial m} - \frac{c_\theta^2}{r} \sin\phi = -\frac{1}{\rho}\frac{\partial p}{\partial m} + F_m \,, \tag{A.1}$$

in stream surface normal direction

$$\frac{c_m^2}{r_c} - \frac{c_\theta^2}{r} \cos\phi = -\frac{1}{\rho}\frac{\partial p}{\partial n} + F_n \,, \tag{A.2}$$

and in the circumferential direction

$$\frac{c_m}{r}\frac{\partial (r c_\theta)}{\partial m} = F_\theta \,. \tag{A.3}$$

The energy equation for steady adiabatic flow is

$$H = h + \frac{c^2}{2} \tag{A.4}$$

where H is stagnation enthalpy. The velocity is $c^2 = c_m^2 + c_\theta^2$, and $c_n = 0$ by definition. Putting the velocity into Equation A.4 we get

$$dh = dH - c_m dc_m - c_\theta dc_\theta \,. \tag{A.5}$$

The Clausius-Gibbs relation is

$$\frac{1}{\rho} dp = dh - T ds \,. \tag{A.6}$$

Putting the Clausius-Gibbs relation into the energy equation we get

$$\frac{1}{\rho} dp = dH - c_m dc_m - c_\theta dc_\theta - T ds \,. \tag{A.7}$$

The derivatives to the l-line are

$$
\begin{aligned}
\frac{d}{dl} &= \frac{dn}{dl}\frac{\partial}{\partial n} + \frac{dm}{dl}\frac{\partial}{\partial m} \\
&= \cos(\phi-\gamma)\frac{\partial}{\partial n} + \sin(\phi-\gamma)\frac{\partial}{\partial m}\,.
\end{aligned}
\tag{A.8}
$$

That is

$$
\frac{\partial}{\partial n} = \frac{1}{\cos(\phi-\gamma)}\frac{\partial}{\partial l} - \tan(\phi-\gamma)\frac{\partial}{\partial m}\,. \tag{A.9}
$$

Adding Equations A.7 and A.1 together

$$
\begin{aligned}
c_m\frac{\partial c_m}{\partial m} - \frac{c_\theta^2}{r}\sin\phi &= -\frac{dH - c_m dc_m - c_\theta dc_\theta - T ds}{\partial m} + F_m \\
&= -\frac{dH}{dm} + c_m\frac{dc_m}{dm} + c_\theta\frac{dc_\theta}{dm} + T\frac{ds}{dm} + F_m\,.
\end{aligned}
\tag{A.10}
$$

That is

$$
-\frac{c_\theta^2}{r}\sin\phi = -\frac{dH}{dm} + c_\theta\frac{dc_\theta}{dm} + T\frac{ds}{dm} + F_m\,. \tag{A.11}
$$

Put Equation A.7 into Equation A.2

$$
\begin{aligned}
\frac{c_m^2}{r_c} - \frac{c_\theta^2}{r}\cos\phi &= -\frac{dH - c_m dc_m - c_\theta dc_\theta - T ds}{\partial n} + F_n \\
&= -\frac{dH}{dn} + c_m\frac{dc_m}{dn} + c_\theta\frac{dc_\theta}{dn} + T\frac{ds}{dn} + F_n\,.
\end{aligned}
\tag{A.12}
$$

We can now eliminate the derivatives with respect to n using Equation A.9

$$
\begin{aligned}
\frac{c_m^2}{r_c} - \frac{c_\theta^2}{r}\cos\phi = &- \frac{1}{\cos(\phi-\gamma)}\frac{\partial H}{\partial l} + \tan(\phi-\gamma)\frac{\partial H}{\partial m} \\
&+ \frac{1}{\cos(\phi-\gamma)}c_m\frac{\partial c_m}{\partial l} - \tan(\phi-\gamma)c_m\frac{\partial c_m}{\partial m} \\
&+ \frac{1}{\cos(\phi-\gamma)}c_\theta\frac{\partial c_\theta}{\partial l} - \tan(\phi-\gamma)c_\theta\frac{\partial c_\theta}{\partial m} \\
&+ \frac{1}{\cos(\phi-\gamma)}T\frac{\partial s}{\partial l} - \tan(\phi-\gamma)T\frac{\partial s}{\partial m} + F_n\,.
\end{aligned}
\tag{A.13}
$$

Adding together Equation A.13 and Equation A.11 $\frac{\sin(\phi-\gamma)}{\cos(\phi-\gamma)}$ we get

$$\begin{aligned}\frac{c_m^2}{r_c} - \frac{c_\theta^2}{r}\cos\phi - \frac{c_\theta^2}{r}\frac{\sin(\phi-\gamma)}{\cos(\phi-\gamma)}\sin\phi = & -\frac{1}{\cos(\phi-\gamma)}\frac{\partial H}{\partial l} + \tan(\phi-\gamma)\frac{\partial H}{\partial m} \\ & + \frac{1}{\cos(\phi-\gamma)}c_m\frac{\partial c_m}{\partial l} - \tan(\phi-\gamma)c_m\frac{\partial c_m}{\partial m} \\ & + \frac{1}{\cos(\phi-\gamma)}c_\theta\frac{\partial c_\theta}{\partial l} - \tan(\phi-\gamma)c_\theta\frac{\partial c_\theta}{\partial m} \\ & + \frac{1}{\cos(\phi-\gamma)}T\frac{\partial s}{\partial l} - \tan(\phi-\gamma)T\frac{\partial s}{\partial m} + F_n \\ & + \frac{\sin(\phi-\gamma)}{\cos(\phi-\gamma)}\left(-\frac{dH}{dm} + c_\theta\frac{dc_\theta}{dm} + T\frac{ds}{dm} + F_m\right).\end{aligned}$$

Isolating $c_m\frac{\partial c_m}{\partial l}$ we get

$$\begin{aligned}c_m\frac{\partial c_m}{\partial l} = & \cos(\phi-\gamma)\frac{c_m^2}{r_c} - \cos(\phi-\gamma)\frac{c_\theta^2}{r}\cos\phi - \frac{c_\theta^2}{r}\sin(\phi-\gamma)\sin\phi + \frac{\partial H}{\partial l} \\ & - \sin(\phi-\gamma)\frac{\partial H}{\partial m} + \sin(\phi-\gamma)c_m\frac{\partial c_m}{\partial m} - c_\theta\frac{\partial c_\theta}{\partial l} + \sin(\phi-\gamma)c_\theta\frac{\partial c_\theta}{\partial m} \\ & - T\frac{\partial s}{\partial l} + \sin(\phi-\gamma)T\frac{\partial s}{\partial m} - \cos(\phi-\gamma)F_n \\ & + \sin(\phi-\gamma)\left(\frac{dH}{dm} - c_\theta\frac{dc_\theta}{dm} - T\frac{ds}{dm} - F_m\right).\end{aligned}$$

Combining (and remembering that $\cos(x-y)\cos x + \sin(x-y)\sin x = \cos y$)

$$\begin{aligned}c_m\frac{\partial c_m}{\partial l} = & \sin(\phi-\gamma)c_m\frac{\partial c_m}{\partial m} + \cos(\phi-\gamma)\frac{c_m^2}{r_c} - \cos(\gamma)\frac{c_\theta^2}{r} \\ & + \frac{\partial H}{\partial l} - T\frac{\partial s}{\partial l} - c_\theta\frac{\partial c_\theta}{\partial l} - \cos(\phi-\gamma)F_n - \sin(\phi-\gamma)F_m.\end{aligned}$$

We can now see that

$$\cos\gamma\frac{c_\theta^2}{r} + c_\theta\frac{dc_\theta}{dl} = \left[\cos\gamma = \frac{dr}{dl}\right] = \frac{c_\theta^2}{r}\frac{dr}{dl} + c_\theta\frac{dc_\theta}{dl} = \frac{c_\theta}{r}\frac{d(rc_\theta)}{dl}. \tag{A.14}$$

The radial equilibrium equation is

$$\begin{aligned}c_m\frac{\partial c_m}{\partial l} = & \sin(\phi-\gamma)c_m\frac{\partial c_m}{\partial m} + \cos(\phi-\gamma)\frac{c_m^2}{r_c} - \frac{c_\theta}{r}\frac{d(rc_\theta)}{dl} \\ & + \frac{dH}{dl} - T\frac{ds}{dl} - \sin(\phi-\gamma)F_m - \cos(\phi-\gamma)F_n.\end{aligned} \tag{A.15}$$

Special Cases - Forced Vortex Flow

Now we will derive a special case of radial equilibrium called Forced Vortex Flow, which behaves as a solid-body rotation. At the entry to the rotor it is assumed that H and s

are constant; that is

$$\nabla s = 0\,,$$
$$\nabla H = 0\,.$$

It is further assumed that the circumferential velocity before the blade is proportional to the radius

$$c_{u1} = K_1 r\,.$$

Assumptions:

- Streamlines have no curvature: $(\phi - \gamma) = 0$ and radius of the curvature aims at infinity and $dl = dr$.
- Bladeless channel: $F_m = F_n = 0$.

Equation A.15 simplifies to

$$c_m \frac{dc_{m1}}{dr} = - \frac{c_{u1}}{r} \frac{d(rc_{u1})}{dr} \tag{A.16}$$
$$= - \frac{K_1 r}{r} \frac{d(rK_1 r)}{dr} = -2K_1^2 r \frac{dr}{dr}\,. \tag{A.17}$$

That is

$$c_{m1} dc_{m1} = -2K_1^2 r dr\,. \tag{A.18}$$

Integrating we get that

$$\int c_{m1} dc_{m1} = -2K_1^2 \int r dr$$
$$\frac{1}{2} c_{m1}^2 = -2K_1^2 \left(\frac{1}{2} r^2 \right) + \text{constant}\,.$$

That is

$$c_{m1}^2 = -2K_1^2 r^2 + K_a \tag{A.19}$$

where K_a is a constant. Next we find the radial distribution for c_{m2} and c_{u2}. Assume that $r = r_2 = r_1$. That means that $U = U_2 = U_1$. We then get

$$c_{u2} = \frac{K_H}{\Omega r} + K_1 r\,. \tag{A.20}$$

Using equation A.16 we get

$$c_{m2} = -4 \frac{K_H K_1}{\Omega} \ln r - 2K_1^2 r^2 + K_2 \tag{A.21}$$

where

$$K_H = H_2 - H_1 = U_2 c_{u2} - U_1 c_{u1}\,. \tag{A.22}$$

Note: when $r_2 \neq r_1$ then

$$c_{u2} = \frac{1}{r_2} \left(\frac{K_H}{\Omega} + K_1 r_1^2 \right) \tag{A.23}$$

and

$$c_{m2}\frac{dv_{m2}}{dr_2} = -\frac{c_{u2}}{r_2}\frac{d}{dr_2}\left(\frac{K_H}{\Omega} + K_1 r_1^2\right) . \tag{A.24}$$

Integrating we get

$$c_{m2}^2 = -2\frac{c_{u2}}{r_2}\left(\frac{K_H}{\Omega} + K_1 r_1^2\right) + K_2 . \tag{A.25}$$

Part II

Appended Papers A–C

Paper A

Conceptual Design of a Mid-Sized, Semi-closed oxy-fuel combustion combined cycle

Paper B

Multicriteria Optimization of Conceptual Compressor Aerodynamic Design

Paper C

Single and Twin-Shaft Oxy-Fuel Gas Turbine Design in a Mid-Size Semi-Closed Oxy-Fuel Combustion Combined Cycle

Paper D

A Comparative Analysis of Two Competing Mid-Size Oxy-Fuel Combustion Cycles